CREDIBILITY INTERVAL DESIGN FOR COVID19 REPRODUCTION NUMBER FROM NONSMOOTH LANGEVIN-TYPE MONTE CARLO SAMPLING

Hugo Artigas, Barbara Pascal, Gersende Fort, Patrice Abry, Nelly Pustelnik

Credibility interval Design for Covid19 Reproduction Number from Nonsmooth Langevin-type Monte Carlo sampling

Hugo Artigas
Ecole Polytechnique, Paris, France

Barbara Pascal
Univ. Lille, CNRS, Centrale Lille, UMR 9189 CRIStAL,
barbara.pascal@univ-lille.fr

Gersende Fort
CNRS, Institut de Mathématiques de Toulouse, France
gersende.fort@math.univ-toulouse.fr

Patrice Abry
CNRS, ENS de Lyon, France
patrice.abry@ens-lyon.fr

Nelly Pustelnik
CNRS, ENS de Lyon, France,
INMA, UCLouvain, Belgium,
nelly.pustelnik@ens-lyon.fr

***Abstract*—Monitoring the Covid19 pandemic is critical to design sanitary policies. Recently, reliable estimates of the pandemic reproduction number were obtained from a nonsmooth convex optimization procedure designed to fit epidemiology requirements and to be robust to the low quality of the data (outliers, pseudo-seasonalities, ...). Applied to daily new infection counts made public by National Health Agencies and centralized by Johns Hopkins University, robust estimates of the reproduction number for 200+ countries are updated and published every day. To further improve estimation procedures and also, and mostly, increase their usability by epidemiologists, the present work exploits the Bayesian paradigm and derives a new Monte Carlo method to sample from a nonsmooth convex a posteriori distribution. This new sampler stems from an original combination of the Langevin Monte Carlo algorithm with Proximal operators. Its relevance and practical efficiency to produce meaningful credibility intervals for the Covid19 reproduction number are assessed from several indices quantifying the statistics of the Monte Carlo chains, and making use of real daily new infection counts.**

I. Introduction

Context. Monitoring the time evolution of the Covid19 pandemic constitutes a critical stake to design counter measures. Pandemic intensity is often assessed by the reproduction number, R, that quantifies the number of second infections stemming from one same primary infection (cf., e.g., [1]–[5]). The online and daily estimate of R turned however extremely difficult during the Covid19 pandemic, mostly because of issues most countries faced in collecting reliable daily new infection counts yielding low-quality data (missing counts, outliers, seasonalities, ...). Therefore, assessing the confidence that can be granted to point estimates is a critical and difficult challenge, motivating the present work.

Related works. While refined pandemic assessment can efficiently be achieved when the pandemic has passed from elaborated compartmental models and Bayesian estimates (cf., e.g., [6], [7]), recently it has been shown that within pandemic, reliable epidemic intensity estimates can be obtained from nonsmooth convex optimization procedures [8], [9]. The functional to minimize is built from the epidemic propagation model proposed in [5], whose quality is to focus on a unique parameter, the reproduction number R, while preserving the key epidemic propagation feature, the so-called *serial interval function* Φ, that quantifies the probability that symptoms today are caused by infection in the past few days. With additional temporal regularity and positivity contraints in the functional, the procedure in [8], [9] delivers epidemiologically realistic estimates that are robust to the low quality of the data. It does not however provide assessment of credibility intervals (CI), an issue what we intend to address here.

H. Artigas and G. Fort are partly funded by the *Fondation Simone et Cino Del Duca, Institut de France* . P. Abry is partially supported by Grant 80PRIME-2021 CNRS.

Goals, contributions and outline. The goal of the present work is to explore the potential of Langevin-type stochastic sampling schemes to produce CI for the evolution of the Covid19 reproduction number R. To that end, the pandemic model in [5] and the one in [8], [9] are first recast into a Bayesian framework, with careful analysis and writing of the corresponding a posteriori distribution (cf. Section II). The core methodological contribution is detailed in Section III: The *Proximal-Gradient dual* stochastic sampling scheme, refining the classical Metropolis Adjusted Langevin Algorithm, is devised to sample a generic class of a posteriori distributions, including the one introduced in Section II. The originality of the proposed sampler is to account for the difficulties stemming from the specificities of the a posteriori distributions considered here.

To assess the relevance of the proposed sampler in producing CI for R, and compare it against simpler *Random Walk*-type samplers, indices quantifying the statistics of the sampled *chains* are defined in Section IV. They are measured on real Covid19 data, consisting of daily infection counts reported by the National Health Authorities of countries around the world, collected and made available by the Johns Hopkins University (cf. Section IV). The practical usability of the sampling strategies and of the achieved CI is discussed both from a technical and epidemiology surveillance perspectives, using Covid19 data from several countries and different time periods.

II. Reproduction number Bayesian model

The pandemic model below elaborates on the one proposed in [5] in order to account for the low quality of the data as detailed and motivated in [9]. In this work, this model is recast into a Bayesian framework. The statistical model associated with the T observations $\mathbf{Z} = (\mathsf{Z}_1, \ldots, \mathsf{Z}_T)^\top \in \mathbb{N}^T$, consisting of new daily infection counts, is indexed by the unknown

$$\theta := (\mathbf{R}, \mathbf{O}) = (\mathsf{R}_1, \ldots, \mathsf{R}_T, \mathsf{O}_1, \ldots, \mathsf{O}_T) \in (\mathbb{R}_+)^T \times \mathbb{R}^T$$

with R_t the reproduction number at time t and O_t the *outliers* modeling the low quality of the data at time t . For any θ, the distribution of Z_t given the past $\mathsf{Z}_1, \ldots, \mathsf{Z}_{t-1}$ and initial values $(\mathsf{Z}_{-\tau_\phi+1}, \cdots, \mathsf{Z}_0)$ is a Poisson distribution with intensity

$$p_t(\theta) := \mathsf{R}_t \sum_{u=1}^{\tau_\phi} \Phi_u \mathsf{Z}_{t-u} + \mathsf{O}_t \ , \tag{1}$$

where the *serial interval function* $(\Phi_u)_{1 \le u \le \tau_\phi}$ accounts for epidemiological mechanisms: It quantifies the random delays between the onset of symptoms in a primary case and in secondary cases [5],

[6], [10]. $(\Phi_u)_{1\le u\le \tau_\phi}$ is assumed known and following [11], [12], it is classically modeled by a Gamma distribution truncated over $\tau_\phi = 26$ days with mean and standard deviation of 6.6 and 3.5 days. By convention, a Poisson distribution with null intensity is the Dirac mass at zero. This implies that the negative log-likelihood of the observations $\mathbf{Z}$ is given by ($0 \ln 0 = 0$ by convention)

$$f(\theta) := \begin{cases} -\sum_{t=1}^{T} \left(\mathsf{Z}_t \ln p_t(\theta) - p_t(\theta)\right) & \text{if } \theta \in \mathcal{D}, \\ +\infty & \text{otherwise,} \end{cases} \tag{2}$$

finite on the measurable set

$$\begin{aligned} \mathcal{D} := &\{\theta \in (\mathbb{R}_+)^T \times \mathbb{R}^T : p_t(\theta) > 0 \text{ for } t \text{ s.t. } \mathsf{Z}_t > 0\} \\ &\cup \{\theta \in (\mathbb{R}_+)^T \times \mathbb{R}^T : p_t(\theta) \ge 0 \text{ for } t \text{ s.t. } \mathsf{Z}_t = 0\} \,. \end{aligned} \tag{3}$$

Interpreting the regularity constraints in [9], the negative logarithm of the a priori distribution of θ defined on $(\mathbb{R}_+)^T \times \mathbb{R}^T$ is [1]

$$g(\theta) := \lambda_{\mathrm{R}} \|\mathsf{D}_2 \mathbf{R}\|_1 + \lambda_{\mathrm{O}} \|\mathbf{O}\|_1 \,; \tag{4}$$

$\|\cdot\|_1$ denotes the L^1-norm. D_2 is the discrete-time second order derivative $(T-2) \times T$ matrix:

$$\mathsf{D}_2 := \frac{1}{\sqrt{6}} \begin{bmatrix} 1 & -2 & 1 & 0 & 0 & \dots & 0 \\ 0 & 1 & -2 & 1 & 0 & \dots & 0 \\ \dots & & & & & & \dots \\ 0 & \dots & & & 1 & -2 & 1 \end{bmatrix} , \tag{5}$$

with normalized rows, and $\lambda_{\mathrm{R}}, \lambda_{\mathrm{O}}$ are (fixed) positive *regularization hyperparameters*, balancing the strengths of the different constraints one against the others and against the likelihood. Under the a priori distribution, $\mathbf{R}$ and $\mathbf{O}$ are independent and distributed resp. as a (non stationary) Laplace AR(2) process and a Laplace distribution. Even if the optima of the a priori distribution satisfy $\mathsf{D}_2\mathbf{R} = 0$ and $\mathbf{O} = 0$, for samples $(\mathbf{R}, \mathbf{O})$ from the a priori distribution, neither $\mathsf{D}_2\mathbf{R}$ not $\mathbf{O}$ are sparse.

Combining the likelihood (2) and the prior (4) leads to the a posteriori density with respect to the Lebesgue measure:

$$\pi(\theta) := \exp\left(-f(\theta) - g(\theta)\right) \mathbb{1}_{\mathcal{D}}(\theta) \,, \tag{6}$$

where $\mathbb{1}_{\mathcal{D}}$ is the $\{0,1\}$-valued indicator function of $\mathcal{D}$. Up to an additive constant, the negative log-likelihood of a Poisson variable Z_t at θ is the Kullback-Leibler distance $d_{\mathrm{KL}}(\mathsf{Z}_t | p_t(\theta))$ between Z_t and $p_t(\theta)$. The negative log-density $-\ln\pi$ is the criterion minimized in [9] for the reconstruction of θ. It is proved in [9], [13] that when $\sum_{u=1}^{\tau_\phi} \Phi_u \mathsf{Z}_{t-u}$ is positive for at least two values $t_\star, t_{\star\star}$, a minimizer of $-\ln\pi$ exists and the set of the minimizers is included in a level set $\{\theta : f(\theta) = f_*\}$ of f (and thus, of g). The a priori distribution implies that the R part of the optima of $\ln\pi$ cannot vary too much across successive days – so that epidemiologists can extract local trends indicating whether the pandemic is increasing or decreasing.

III. Nonsmooth Langevin Monte Carlo samplers

When the posterior distribution is known up to a normalizing constant (as in Section II), estimation through the Bayesian paradigm entails the use of numerical tools such as Markov Chain Monte Carlo (MCMC) samplers designed to define an empirical distribution approximating the posterior distribution. The computation of α-credibility regions (see, e.g., [14, chapter 5]) or of Bayesian estimators such as the posterior mean, the median or the Maximum A Posteriori (MAP), follows from a Monte Carlo (MC) approximation.

[1] In the Bayesian setting, the distributions are often defined up to a multiplicative constant. We adopt this convention here.

In this work, we propose original MCMC samplers targeting a generic density π of the form (6) and satisfying A1-A2.

Assumptions on the target density π.

A1. *f and g are finite on a measurable set $\mathcal{D}$ and f is continuously differentiable on the interior of $\mathcal{D} \subseteq \mathbb{R}^d$.*

A2. *g is blockwise: for $j \in \{1, \dots, J\}$, there exist matrices $\mathsf{A}_j \in \mathbb{R}^{c_j \times d_j}$, with $c_j \le d_j$, and proper, convex, lower semi-continuous functions $g_j \colon \mathbb{R}^{c_j} \to]-\infty, +\infty]$ such that $\sum_{j=1}^{J} d_j = d$ and*

$$\forall \theta := (\theta_1, \dots, \theta_J) \in \mathbb{R}^{d_1} \times \dots \times \mathbb{R}^{d_J}, \quad g(\theta) = \sum_{j=1}^{J} g_j(\mathsf{A}_j \theta_j) \,,$$

where, for each $j \in \{1, \dots, J\}$, (i) the proximal operator[2] of g_j possesses a closed-form expression[3], (ii) A_j is full rank, so that it can be augmented into an invertible matrix $\overline{\mathsf{A}}_j \in \mathbb{R}^{d_j \times d_j}$, (iii) g_j extends into $\bar{g}_j \colon \mathbb{R}^{d_j} \to]-\infty, +\infty]$ such that $\forall \theta_j$, $g_j(\mathsf{A}_j\theta_j) = \bar{g}_j(\overline{A}_j \theta_j)$.

A1 requires the differentiability of f but not the Lipschitz property for its gradient; A2 does not assume that the proximal operator of g has a closed-form expression.

Example. For the target density π defined in Section II, both A 1 and A 2 are valid. We have $d = 2T$, $J = 2$, $\theta_1 = \mathbf{R}$, $\theta_2 = \mathbf{O}$, $g_1 = \lambda_{\mathrm{R}} \|\cdot\|_1$, $g_2 = \lambda_{\mathrm{O}} \|\cdot\|_1$, $\mathsf{A}_1 = \mathsf{D}_2$ (see (5)), and $\mathsf{A}_2 = \mathsf{I}$, the identity matrix. A_1 can be augmented in many different ways, among which:

$$\overline{\mathsf{D}}_2 := \begin{bmatrix} 1 & 0 & 0 & \cdots & 0 \\ -2/\sqrt{5} & 1/\sqrt{5} & 0 & \cdots & 0 \\ & & \mathsf{D}_2 & & \end{bmatrix} . \tag{7}$$

Another possibility is $\overline{\mathsf{D}}_o$, obtained from $\overline{\mathsf{D}}_2$ by making its first two rows orthogonal, and orthogonal to the rows of D_2. Then, $\bar{g}_1 = \lambda_{\mathrm{R}} \|(\cdot)_{3:T}\|_1$, computed only on components 3 to T, and $\bar{g}_2 = g_2$.

Metropolis Adjusted Langevin Algorithm (MALA) sampler and its limitations. If $-\ln\pi = f$ (i.e., $g = 0$) is a smooth function on $\mathcal{D}$, a popular MCMC sampler which takes benefit of a first order knowledge of π, relies on Langevin dynamics, stemming from *tempered Langevin diffusion* [16]. Given a $d \times d$ matrix Γ and a positive step size γ chosen by the user, at each iteration $\#(n+1)$ starting from the current point θ^n, a jump is proposed to the point

$$\theta^{n+\frac{1}{2}} := \theta^n - \gamma \Gamma \Gamma^\top \nabla f(\theta^n) + \sqrt{2\gamma} \Gamma \, \xi^{n+1} \,, \tag{8}$$

where $\xi^{n+1} \sim \mathcal{N}_d(0, \mathsf{I})$ is a standard $\mathbb{R}^d$-valued Gaussian distribution. $\mathsf{A}^\top$ denotes the transpose of the matrix A. This proposal is accepted ($\theta^{n+1} = \theta^{n+\frac{1}{2}}$) or rejected ($\theta^{n+1} = \theta^n$) through a Metropolis mechanism, and this yields the *Metropolis Adjusted Langevin Algorithm* (MALA, [17]). The idea of MALA methods is to drift the proposed moves towards areas of high probability under π, by using the information provided by $\nabla \ln \pi$.

Proximal-Gradient dual sampler (`PGdual`). In the present work, $-\ln\pi$ is not smooth (see A 2): this calls for the use of Proximal Langevin-based MC methods. The literature provides examples of MC samplers combining a Langevin approach and a Proximal approach (see, e.g., [18]–[25]) but none of these algorithms directly apply to the framework A 1-A 2. Indeed, the density π may be positive for non-sparse $(\mathsf{D}_2\mathbf{R}, \mathbf{O})$. Further, A2 assumes that g_j has

[2] $\mathrm{prox}_g(y) := \mathrm{argmin}_{x \in \mathbb{R}^\ell} (g(x) + \|x - y\|^2/2)$ is well-defined for any proper, convex, lower semi-continuous function $g : \mathbb{R}^\ell \to]-\infty, +\infty]$. $\|\cdot\|$ denotes the Euclidean norm in $\mathbb{R}^\ell$.

[3] See [15] to have an exhaustive list of known proximal operators.

an explicit proximal operator for any $j \in \{1, \dots, J\}$ which does not imply that this holds true for g, notably when g involves a linear operator, e.g., in (4). Finally, we want to promote a method which takes benefit of both the blockwise separable expression of g and the full rank property of matrices A_j by computing the proximal operator separately on each range space of $\bar{\mathsf{A}}_j$. These limitations led us to propose the following original and general Proximal-Gradient dual (`PGdual`) Algorithm (sketched in Algorithm 1), which is among the Metropolis-Hastings samplers with Gaussian proposal; the main originality is the definition of the drift term. At iteration $\#(n+1)$, a candidate is proposed, whose block $\#j$ is

$$\theta_j^{n+\frac{1}{2}} := \mu_j(\theta^n) + \sqrt{2\gamma_j}\Gamma_j\,\xi_j^{n+1}\,, \quad \forall\, j \in \{1, \dots, J\}\,, \quad (9)$$

where $\xi_j^{n+1} \sim \mathcal{N}_{d_j}(0, \mathsf{I})$ and

$$\mu_j(\theta) := \overline{\mathsf{A}}_j^{-1}\mathrm{prox}_{\gamma_j \bar{g}_j}\left(\overline{\mathsf{A}}_j\theta_j - \gamma_j \overline{\mathsf{A}}_j^{-\top}\nabla_j f(\theta)\right)\,; \quad (10)$$

∇_j denotes the gradient with respect to the block $\#j$ and $\mathsf{A}^{-\top}$ is the inverse of $\mathsf{A}^\top$. $\mu_j(\theta^n)$ performs a proximal-gradient iteration associated to a part of the original composite function in the *dual* space, consisting in the range of the matrix $\bar{\mathsf{A}}_j$; then sends each block $\#j$ back in the direct space through the mapping $\bar{\mathsf{A}}_j^{-1}$. Formally, $-\ln\pi$ transferred in the dual space reads

$$(\tilde{\theta}_1, \dots, \tilde{\theta}_J) \mapsto f(\bar{\mathsf{A}}_1^{-1}\tilde{\theta}_1, \dots, \bar{\mathsf{A}}_J^{-1}\tilde{\theta}_J) + \sum_{j=1}^{J} \bar{g}_j(\tilde{\theta}_j).$$

Introducing $q_j(\theta, \theta_j')$ the Gaussian kernel on $\mathbb{R}^{d_j}$ centered at $\mu_j(\theta)$, with covariance matrix $2\gamma_j\Gamma_j\Gamma_j^\top$ and evaluated at θ_j', the acceptance-rejection (AR) step defined Line 5 makes Algorithm 1 to have π as unique invariant distribution.

There is a parallel between the preconditioned gradient appearing in the drift term (10) of the proposed point (9), and the scaled Langevin dynamics (8). For this reason, we advocate $\Gamma_j = \bar{\mathsf{A}}_j^{-1}$ for any j, whatever the proximal operator is.

Our recent work [13] shows how to apply `PGdual` in a more general setting than A 2, when there are many penalty terms for each block $\#j$. It also discusses how `PGdual` is related to other proximal-gradient based extensions of the MALA sampler.

Example (to follow). For π defined in Section II, the μ_j's are

$$\mu_1(\theta) := \overline{\mathsf{D}}^{-1}\,\mathrm{prox}_{\lambda_{\mathrm{R}}\|(\cdot)_{3:T}\|_1}\left(\overline{\mathsf{D}}\,\mathbf{R} - \gamma_1\overline{\mathsf{D}}^{-\top}\,\nabla_1 f(\theta)\right)\,, \quad (11)$$

$$\mu_2(\theta) := \mathrm{prox}_{\lambda_{\mathrm{O}}\|\cdot\|_1}\left(\mathbf{O} - \gamma_2\nabla_2 f(\theta)\right)\,, \quad (12)$$

where $\overline{\mathsf{D}}$ is a $(T \times T)$ invertible augmentation of D_2, see, e.g., Eq (7).

IV. Credibility intervals from Covid19 data

Covid19 data. The data used here are part of a large data set available from the *Johns Hopkins University*[4], consisting of daily new infection counts for around 200 countries, by National Health Authorities. The focus is here on the evolution of R_t on a realistic time period of $T = 35$ days (5 weeks) of pandemic. To account for the time support of the serial function Φ, we use $\tau_\phi = 26$ additional observations for the initialization $\mathsf{Z}_{-\tau_\phi+1}, \cdots, \mathsf{Z}_0$. Counts from January, 1st 2022 to February, 4th 2022 for Italy are used for the performance assessments (see Figure 1, Figure 2). However, tools and methods proposed here have been applied to numerous countries for various time periods of interest (see, e.g., Figure 3).

MCMC samplers. The proposal mechanisms of `PGdual` are

$$\mathbf{R}^{n+\frac{1}{2}} = \mu_1(\theta^n) + \sqrt{2\gamma_1}\,\overline{\mathsf{D}}^{-1}\xi_1^{n+1}, \mathbf{O}^{n+\frac{1}{2}} = \mu_2(\theta^n) + \sqrt{2\gamma_2}\,\xi_2^{n+1}$$

[4] https://coronavirus.jhu.edu/

Algorithm 1: Proximal-Gradient dual (`PGdual`)

Data: $d_j \times d_j$ matrices Γ_j, $\gamma_j > 0$, $N_{\max} \in \mathbb{N}_\star$, $\theta^0 \in \mathcal{D}$
Result: A $\mathcal{D}$-valued sequence $\{\theta^n, n \in 0, \dots, N_{\max}\}$

1 **for** $n = 0, \dots, N_{\max} - 1$ **do**
2 **for** $j = 1, \dots, J$ **do**
3 Sample $\xi_j^{n+1} \sim \mathcal{N}_{d_j}(0, \mathsf{I})$;
4 Set $\theta_j^{n+\frac{1}{2}} = \mu_j(\theta^n) + \sqrt{2\gamma_j}\Gamma_j\,\xi_j^{n+1}$;
5 Set $\theta^{n+1} = \theta^{n+\frac{1}{2}}$ with probability

$$1 \wedge \frac{\pi(\theta^{n+\frac{1}{2}})}{\pi(\theta^n)}\prod_{j=1}^{J}\frac{q_j(\theta^{n+\frac{1}{2}}, \theta_j^n)}{q_j(\theta^n, \theta_j^{n+\frac{1}{2}})}$$

 and $\theta^{n+1} = \theta^n$ otherwise.

where μ_1, μ_2 are defined by (11), (12). Two versions of `PGdual` are compared: `PGdual Invert` when $\overline{\mathsf{D}} = \overline{\mathsf{D}}_2$, and `PGdual Ortho` when $\overline{\mathsf{D}} = \overline{\mathsf{D}}_o$ (see Section III for the definition of $\overline{\mathsf{D}}_2$ and $\overline{\mathsf{D}}_o$). Further, `PGdual` is compared to the Random Walk (`RW`) sampler, whose proposal mechanism is

$$\mathbf{R}^{n+\frac{1}{2}} = \mathbf{R}^n + \sqrt{2\gamma_1}\,\xi_1^{n+1}, \quad \mathbf{O}^{n+\frac{1}{2}} = \mathbf{O}^n + \sqrt{2\gamma_2}\,\xi_2^{n+1}\,.$$

We also explore the benefit of covariance matrices for the $\mathbf{R}$-part of the Random Walk chains: `RW Invert` and `RW Ortho` correspond to $\mathbf{R}^{n+\frac{1}{2}} = \mathbf{R}^n + \sqrt{2\gamma_1}\,\overline{\mathsf{D}}^{-1}\xi_1^{n+1}$ resp. in the case $\overline{\mathsf{D}} = \overline{\mathsf{D}}_2$ and $\overline{\mathsf{D}} = \overline{\mathsf{D}}_o$; the proposal mechanism for the $\mathbf{O}$-part is as in `RW`. These comparisons will outline the role of the drift terms μ_j, and of the covariance matrix of the Gaussian proposition.

Settings. All chains are run for $N_{\max} = 10^7$ iterations. Except in Figure 1[left], displayed quantities are computed from the Markov path after discarding its first 30% points corresponding to a burn in period. All the curves displayed on Figure 1 and Figure 2 are mean values over 15 independent runs: they start from different points θ^0 obtained by Gaussian perturbations of the intuitive but poor (in terms of value of π) value $\mathbf{R}^{\mathrm{init}} := (1, \dots, 1)^\top$ and $\mathbf{O}^{\mathrm{init}} := (0, \dots, 0)^\top$. The step size γ_1 is adapted during the burn in period in order to target a mean AR ratio equal to 0.25, and then it is frozen. For fair comparisons among methods, we use here the same target AR ratio which is known to be optimal for Random Walk algorithms (see, e.g., [26]; similar results for nonsmooth Langevin samplers do not exist). We set $(\lambda_{\mathrm{R}}, \lambda_{\mathrm{O}}) = (3.5\,\sigma_{\mathbf{Z}}\sqrt{6}/4, 0.05)$ as in [9], where $\sigma_{\mathbf{Z}}$ is the standard deviation of the data set $\mathbf{Z}$. In addition, $\gamma_2 = \gamma_1$ for `RW` and for the other algorithms, $\gamma_2 = \gamma_1(\lambda_{\mathrm{R}}/\lambda_{\mathrm{O}})^2$.

MCMC performance. Figure 1[top] displays the evolution of the normalized distance to the MAP $\widehat{\mathbf{R}}$ along iterations: $n \mapsto \|\mathbf{R}^n - \widehat{\mathbf{R}}\|/\|\widehat{\mathbf{R}}\|$ for the five MCMC samplers. Figure 1[bottom] displays the evolution of the normalized log-density along iterations $n \mapsto (\ln\pi(\theta^n) - \max\ln\pi)/(\ln\pi(\theta^0) - \max\ln\pi)$ for the five MCMC samplers. $\widehat{\mathbf{R}}$ is computed by the method in [9]. Figure 2 compares the samplers through two criteria related to the convergence: the lag-k auto-correlation function (ACF) of a Markov chain with initial distribution π - it is related to the effective sample size of a Markov chain (see [27]); and the Gelman-Rubin statistic (GR, [28]). The ACF plots are obtained as mean absolute values of the $2T$ real valued ACF of $(\mathsf{R}_t, \mathsf{O}_t)_{1 \le t \le T}$. GR can be read as a ANOVA-type criterion, reaching an optimal value of one when the different paths are homogeneous.

These plots show that: *(i)* `RW` has a poor behavior compared to the other samplers, thus illustrating the role of the drift and the

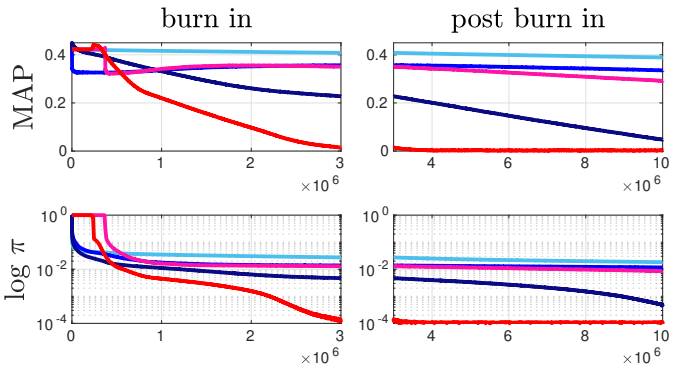

Fig. 1. **MCMC sampler performance.** `RW` in light blue, `RW Invert` in blue and `RW Ortho` in dark blue; `PGdual Invert` in pink and `PGdual Ortho` in red. During the burn in period [left] and after [right], evolution of the distance to the MAP along iterations [top] and to $\max \ln \pi$ along iterations [bottom].

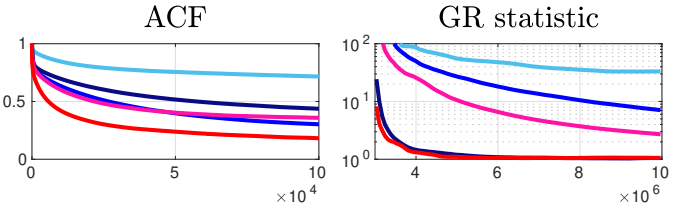

Fig. 2. **MCMC sampler performance.** `RW` in light blue, `RW Invert` in blue and `RW Ortho` in dark blue; `PGdual Invert` in pink and `PGdual Ortho` in red. [left] Mean absolute value of the ACF vs the first 10^5 lags. [right] The GR statistic vs iterations.

covariance matrix $\overline{\mathsf{D}}^{-1}\overline{\mathsf{D}}^{-\top}$ in the efficiency of the samplers: `RW` fails to converge before $N_{\max}$ iterations contrary to `PGdual Ortho`. Indeed, from the results on Figure 1 and Figure 2: the distance to $\widehat{\mathbf{R}}$ and the evolution of $\ln \pi$ along the path show that `RW` moves slowly to high density regions thus being not efficient at all in the exploration of the target distribution π; in addition, its ACF decreases to 0 very slowly and there is a strong heterogeneity between the 15 runs of this method (see the GR statistic). *(ii)* The behavior of the Random Walk based methods is improved thanks to a genuine choice of the covariance matrix: `RW Invert` and - with a stronger evidence - `RW Ortho` take benefit of correlated Gaussian noises for the $\mathbf{R}$-part of the chain. *(iii)* For the drift part of the proposal mechanism, there is a gain in using first order information on $\ln \pi$: if `RW Invert` and `PGdual Invert` have a similar behavior on Figure 1 and Figure 2[left] with a slight advantage for `PGdual Invert`, `PGdual Ortho` is definitely better than `RW Ortho` and than all the other methods. When the adapted step size is small enough, it has the highest speed of convergence to the optimum of $\ln \pi$; at the end of the burn in period, it reached high density regions; it provides the faster decaying rate of the ACF; its GR statistic converges rapidly to the optimal value.

Credibility intervals. Let us further illustrate the relevance of CI-based estimations for R and O. For practical purposes, the CIs for O are translated into CIs for the denoised counts $\mathbf{Z}^{(D)}$ by subtraction to the original counts $\mathbf{Z}$: intuitively, $\mathbf{Z}^{(D)} = \mathbf{Z} - \mathbf{O}$. CIs are reported for `PGdual Ortho` only - since shown above to yield the best performance - for several countries and various time periods of interest. The 95% CIs are obtained from the empirical quantiles 0.025 and 0.975 of the Markov paths. In Figure 3, for each country, the top plot shows the daily counts $\mathbf{Z}$ (black) with the CI estimates of

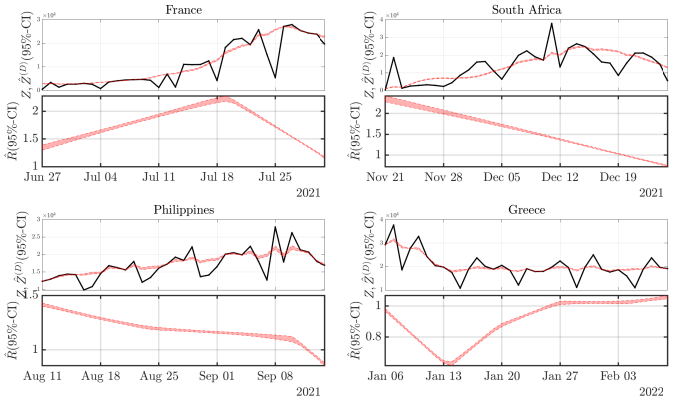

Fig. 3. **Credibility intervals** for different countries and different time periods. For each country, observed counts $\mathbf{Z}$ (black solid lines) and 95% credibility interval denoised counts $\mathbf{Z}^{(D)}$ (red pipe) [top] ; 95% credibility interval estimates for R [Bottom].

the denoised counts $\mathbf{Z}^{(D)}$ (red), while the bottom plot represents the CI estimates for R.

For France, the selected time period was chosen when the 4th pandemic wave started to severely strike the country (mid-june 2021) until reaching $\mathsf{R} \simeq 2$ early July. Figure 3 shows that CIs excluded "$\mathsf{R} < 1$" before the end of June. Early July, the French Health Authorities made the announcement of a mandatory "sanitary pass" for any social activities after Aug. 9th. An immediate and massive vaccination *phase* started in the French population, which yields the *plateau* of the 4th wave, clearly observed in Figure 3 to be reached in the 3rd week of July. CIs further validate a clear decay of R after July 20th, that is, two weeks before the counts of infections actually started to decrease, thus showing the relevance and interest of the CI estimates for R. For the Philippines and South Africa, the periods of late April 2021 and late August 2021 correspond to massive strikes of the pandemic. For both countries, Figure 3 confirms that the changes of slopes in R announce a few weeks in advance the maximum of the wave and the start of the decay in new infections. For Greece, the CIs enable to detect with high confidence that "$\mathsf{R} > 1$" since January 27th 2022, which was far from being obvious by directly observing the infection counts.

Estimates and credibility intervals are updated on a regular basis and made available for the current period and for France, at perso.math.univ-toulouse.fr/gfort/project/opsimore-2/.

V. Conclusions and Future Works

The present work constitutes a significant step toward the actual use of the tools envisaged in [8], [9] to monitor the reproduction number. Introducing a Bayesian formalism permits to produce reliable credibility intervals for the reproduction number, as well as Bayesian estimators. It relies on an original Proximal-based Langevin MCMC algorithm designed to handle a convex but nonsmooth a posteriori potential $-\ln \pi$, whose nonsmooth part consists of the sum of several terms and which is able to account for the epidemiological model. Satisfactory agreements between credibility intervals and point estimates (MAP, posterior mean, ...), obtained using real Covid19 data, emphasize the reliability of this novel MCMC sampler. Comparisons against other MCMC strategies have further been explored in [29], [30]. Future investigations include the automated data-driven tuning of the design parameters (e.g., step sizes γ_i), and the theoretical derivation of `PGdual` convergence rates which are, to the best of

our knowledge, an open question for many MALA-based samplers designed for nonsmooth target distributions. Performance assessment on realistic synthetic Covid data are under investigation.

REFERENCES

[1] O. Diekmann, J. A. P. Heesterbeek, and J. A. J. Metz, "On the definition and the computation of the basic reproduction ratio R0 in models for infectious diseases in heterogeneous populations," *J. Math. Biol.*, vol. 28, pp. 365–382, 1990.

[2] J. Wallinga and P. Teunis, "Different Epidemic Curves for Severe Acute Respiratory Syndrome Reveal Similar Impacts of Control Measures," *Am. J. Epidemiol.*, vol. 160, pp. 509–516, 2004.

[3] P. van den Driessche and J. Watmough, "Reproduction numbers and sub-threshold endemic equilibria for compartmental models of disease transmission," *Math Biosci*, vol. 180, pp. 29–48, 2002.

[4] T. Obadia, R. Haneef, and P.-Y. Boëlle, "The R0 package: A toolbox to estimate reproduction numbers for epidemic outbreaks," *BMC Medical Inform Decis. Mak.*, vol. 12, p. 147, 2012.

[5] A. Cori, N. M. Ferguson, C. Fraser, and S. Cauchemez, "A new framework and software to estimate time-varying reproduction numbers during epidemics," *Am. J. Epidemiol.*, vol. 178, pp. 1505–1512, 2013.

[6] Q.-H. Liu, M. Ajelli, A. Aleta, S. Merler, Y. Moreno, and A. Vespignani, "Measurability of the epidemic reproduction number in data-driven contact networks," *Proc. Natl. Acad. Sci. U.S.A.*, vol. 115, pp. 12 680–12 685, 2018.

[7] F. Brauer, C. Castillo-Chavez, and Z. Feng, *Mathematical models in epidemiology*. Springer, New York, 2019.

[8] P. Abry et al., "Spatial and temporal regularization to estimate COVID-19 reproduction number $R(t)$: Promoting piecewise smoothness via convex optimization," *PLOS One*, vol. 15, 2020, e0237901.

[9] B. Pascal, P. Abry, N. Pustelnik, S. Roux, R. Gribonval, and P. Flandrin, "Nonsmooth convex optimization to estimate the Covid-19 reproduction number space-time evolution with robustness against low quality data," arXiv 2109.09595, Tech. Rep., 2022.

[10] R. Thompson et al., "Improved inference of time-varying reproduction numbers during infectious disease outbreaks," *Epidemics*, vol. 29, p. 100356, 2019. [Online]. Available: http://www.sciencedirect.com/science/article/pii/S1755436519300350

[11] F. Riccardo et al., "Epidemiological characteristics of COVID-19 cases in Italy and estimates of the reproductive numbers one month into the epidemic," medRxiv:2020.04.08.20056861, 2020. [Online]. Available: https://www.medrxiv.org/content/early/2020/04/11/2020.04.08.20056861

[12] G. Guzzetta et al., "The impact of a nation-wide lockdown on COVID-19 transmissibility in Italy," arXiv:2004.12338 [q-bio.PE], 2020.

[13] G. Fort, B. Pascal, P. Abry, and N. Pustelnik, "Covid19 Reproduction Number: Credibility Intervals by Blockwise Proximal Monte Carlo Samplers," HAL, Tech. Rep., 2022.

[14] C. P. Robert, *The Bayesian choice: a decision-theoretic motivation*. Springer-Verlag, 1994.

[15] G. Chierchia, E. Chouzenoux, P. Combettes, and J.-C. Pesquet, "The proximity operator repository," *http://proximity-operator.net/*.

[16] J. Kent, "Time-Reversible Diffusions," *Adv Appl Probab*, vol. 10, no. 4, pp. 819–835, 1978.

[17] G. O. Roberts and R. L. Tweedie, "Exponential convergence of Langevin distributions and their discrete approximations," *Bernoulli*, vol. 2, pp. 341 – 363, 1996.

[18] M. Pereyra, P. Schniter, E. Chouzenoux, J.-C. Pesquet, J.-Y. Tourneret, A. O. Hero, and S. McLaughlin, "A survey of stochastic simulation and optimization methods in signal processing," *IEEE J. Selected Topics Signal Process.*, vol. 10, pp. 224–241, 2016.

[19] Y. Atchadé, "A Moreau-Yosida approximation scheme for a class of high-dimensional posterior distributions," arXiv: Statistics Theory, Tech. Rep., 2015.

[20] A. Schreck, G. Fort, S. L. Corff, and É. Moulines, "A Shrinkage-Thresholding Metropolis Adjusted Langevin Algorithm for Bayesian Variable Selection," *IEEE J. Selected Topics Signal Process.*, vol. 10, pp. 366–375, 2016.

[21] A. Salim and P. Richtarik, "Primal Dual Interpretation of the Proximal Stochastic Gradient Langevin Algorithm," in *Advances in Neural Information Processing Systems*, H. Larochelle, M. Ranzato, R. Hadsell, M. F. Balcan, and H. Lin, Eds., vol. 33, 2020, pp. 3786–3796.

[22] A. Durmus, E. Moulines, and M. Pereyra, "Efficient Bayesian Computation by Proximal Markov Chain Monte Carlo: When Langevin Meets Moreau," *SIAM J Imaging Sci*, vol. 11, pp. 473–506, 2018.

[23] A. Durmus, S. Majewski, and B. Miasojedow, "Analysis of Langevin Monte Carlo via Convex Optimization," *J. Mach. Learn. Res.*, vol. 20, pp. 73:1–73:46, 2019.

[24] N. Chatterji, J. Diakonikolas, M. I. Jordan, and P. Bartlett, "Langevin Monte Carlo without smoothness," in *Proceedings of the Twenty Third International Conference on Artificial Intelligence and Statistics*, ser. Proceedings of Machine Learning Research, S. Chiappa and R. Calandra, Eds., vol. 108, 2020, pp. 1716–1726.

[25] T. Luu, J. Fadili, and C. Chesneau, "Sampling from Non-smooth Distributions Through Langevin Diffusion," *Methodol Comput Appl Probab*, 2020.

[26] G. Roberts and J. Rosenthal, "Optimal scaling for various Metropolis-Hastings algorithms," *Statistical Science*, vol. 16, pp. 351 – 367, 2001.

[27] C. P. Robert and G. Casella, *Monte Carlo Statistical Methods (Springer Texts in Statistics)*. Berlin, Heidelberg: Springer-Verlag, 2005.

[28] S. Brooks and A. Gelman, "General methods for monitoring convergence of iterative simulations," *J Comput Graph Stat*, vol. 7, pp. 434–455, 1998.

[29] P. Abry, G. Fort, B. Pascal, and N. Pustelnik, "Temporal evolution of the Covid19 pandemic reproduction number: Estimations from Proximal optimization to Monte Carlo sampling," in *IEEE-EMBS Engineering in Medicine and Biology Conference*, Glascow, United Kingdom, 2022.

[30] ——, "Estimation et intervalles de crédibilité pour le taux de reproduction de la Covid19 par échantillonnage Monte Carlo Langevin proximal," in *XXVIIIème Colloque Francophone de Traitement du Signal et des Images*, Nancy, France, 2022.